

Probabilistic Margins for Instance Reweighting in Adversarial Training

Qizhou Wang^{*1}, Feng Liu^{*2}, Bo Han¹, Tongliang Liu³, Chen Gong⁴, Gang Niu⁵, Mingyuan Zhou⁶, and Masashi Sugiyama^{5,7}

¹Department of Computer Science, Hong Kong Baptist University

²DeSI Lab, AAI, University of Technology Sydney

³TML Lab, The University of Sydney

⁴Key Laboratory of Intelligent Perception and Systems for High-Dimensional Information of MoE, Nanjing University of Science and Technology

⁵RIKEN Center for Advanced Intelligence Project (AIP)

⁶IROM Department, McCombs School of Business, The University of Texas

⁷Graduate School of Frontier Sciences, The University of Tokyo

Abstract

Reweighting adversarial data during training has been recently shown to improve adversarial robustness, where data *closer* to the current decision boundaries are regarded as *more critical* and given *larger weights*. However, existing methods measuring the closeness are not very reliable: they are *discrete* and can take only a few values, and they are *path-dependent*, i.e., they may change given the same start and end points with different attack paths. In this paper, we propose three types of *probabilistic margin* (PM), which are *continuous* and *path-independent*, for measuring the aforementioned closeness and reweighting adversarial data. Specifically, a PM is defined as the difference between two *estimated class-posterior probabilities*, e.g., such the probability of the true label minus the probability of the most confusing label given some natural data. Though different PMs capture different *geometric properties*, all three PMs share a negative correlation with the vulnerability of data: data with larger/smaller PMs are safer/riskier and should have smaller/larger weights. Experiments demonstrate that PMs are reliable measurements and PM-based reweighting methods outperform state-of-the-art methods.

1 Introduction

Deep neural networks are susceptible to adversarial examples that are generated by changing natural inputs with malicious perturbation [Du et al., 2021, Gao et al., 2021, Szegedy et al., 2014, Wang et al., 2020a]. Those examples are imperceptible to human eyes but can fool deep models to make wrong predictions with high confidence [Athalye et al., 2018b, Qin et al., 2019]. As deep learning has been deployed in many real-life scenarios and even safety-critical systems [Chen et al., 2020, De Prado, 2018, Litjens et al., 2017, Yang et al., 2021], it is crucial to make such deep models reliable and safe [Finlayson et al., 2019, Kurakin et al., 2017, Zheng et al., 2020]. To obtain more reliable deep models, *adversarial training* (AT) [Athalye et al., 2018a, Madry et al., 2018] was proposed as one of the most effective methodologies against adversary attacks (i.e., maliciously changing natural inputs). Specifically, during AT, they simulate adversarial examples (e.g., generated by *project gradient descent* (PGD) [Andriushchenko and Flammarion, 2020, Madry et al., 2018, Zhang et al., 2020, Wong et al., 2020]) and train a classifier with the simulated adversarial examples [Madry

^{*}Contributed equally.

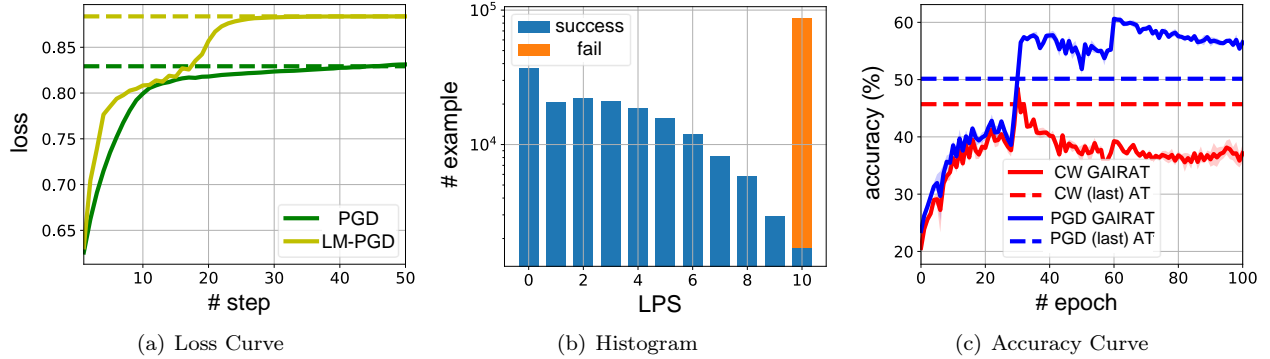


Figure 1: An illustration of the drawbacks of LPS. (a) suggests that LPS might be path-dependent since the vanilla PGD method (PGD) may get stuck at sub-optimal points. Here, we prove the existence of a better (might not be optimal) solution given by *line-search & momentum-PGD* (LM-PGD) (cf. Appendix A). LPSs are 50 and 14 estimated by PGD and LM-PGD, revealing that LPS depends on the adopted attacks. (b) suggests that LPS can take only a few discrete values, and it has a confusing meaning when LPS meets the maximal value. In this case, one can hardly distinguish the non-robust data with LPS being 10 and the safe data that are insensitive to be attacked. (c) shows that the accuracy of GAIRAT (on *CIFAR-10*) will drop significantly when facing CW attacks. The main reason is that LPS is not reliable to measure the distance between data and decision boundaries ((a), (b)). As a result, it makes wrong judgments when assigning weights for non-robust instances.

et al., 2018, Zhang et al., 2020]. Since such a model has seen some adversarial examples during its training process, it can defend against certain adversarial attacks and is more *adversarial-robust* than a classifier only trained with natural data [Bubeck et al., 2019, Cullina et al., 2018, Schmidt et al., 2018].

Recently, researcher have found that over-parameterized deep networks still have the insufficient model capacity, since adversarial training has an overwhelming smoothing effect [Zhang et al., 2021, Pang et al., 2020]. As a result, they proposed *instance-reweighted adversarial training*, where adversarial data should have unequal importance given limited model capacity [Zhang et al., 2021]. Concretely, they suggested that data *close* to decision boundaries are vulnerable to be attacked [Zhang et al., 2019, 2021] and should be assigned large weights during training. To characterize these *geometric properties* of data (i.e., the closeness between data and decision boundaries), Zhang et al. [2021] suggested an estimation in input space, i.e., the *least PGD steps* (LPS), to identify non-robust (easily-be-attacked) data. LPS measures how many steps the PGD method needs to attack natural data successfully. Specifically, LPS is the number of steps to make the adversarial variant of such an instance cross the decision boundaries starting from a natural instance. Based on LPS, they achieved state-of-the-art performance via a general framework termed *geometry-aware instance-reweighted adversarial training* (GAIRAT).

However, existing methods [Fawzi et al., 2018, Ilyas et al., 2019, Tsipras et al., 2019] in measuring geometric properties of data are *path-dependent*, i.e., they may change even given the same start (i.e., a natural example) and end point (i.e., the adversarial variant), and (or) they are *discrete* with only a few valid values (cf. Figure 2). The path-dependency makes the computation

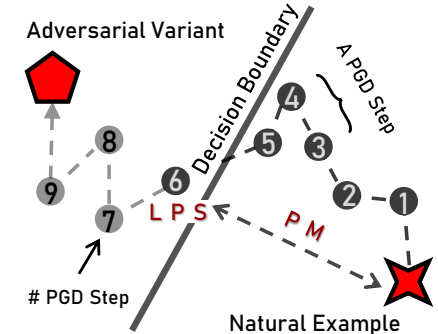


Figure 2: The path-dependency and discreteness of LPS, and the proposed PM in comparison. The PGD methods uses 6 step to find an instance to violate the boundary (i.e., LPS is 6), while PM is continuous to represent the distance.

unstable, where the results may change due to the different attack paths. The discreteness makes the measurement ambiguous since each value would have several (even contradictory) meanings. We take LPS, a representative measurement [Zhang et al., 2021], as an example to demonstrate a path-dependent (Figure 1a) and discrete measurement (Figure 1b). As we can see in Figure 1c, the consequence is non-negligible: although adopting LPS (i.e., GAIRAT) reveals improvement for the PGD-20 attack [Madry et al., 2018], its performance is well below traditional AT regarding a stronger attack method, CW [Carlini and Wagner, 2017].

In this paper, we propose the *probabilistic margin* (PM), which is *continuous* and *path-independent*, for reweighting adversarial data during AT. PM is a geometric measurement from a data point to the closest decision boundary, following the *multi-class margin* [Koltchinskii et al., 2002] in traditional geometry-aware machine learning (e.g., the support vector machine [Cortes and Vapnik, 1995]). Note that, instead of choosing the input space as LPS, PM is defined based on the *estimated class-posterior probabilities* from model outputs, e.g., such the probability of the true label minus the probability of the most confusing label given some natural data. Therefore, PM is computed in a low-dimensional embedding space with normalization, alleviating troubles in comparing data from different classes.

The definition of PM is general, where we consider three specifications, namely, PM^{nat} , PM^{adv} , and PM^{dif} . Therein, PM^{nat} and PM^{adv} are the PM scores regarding natural and adversarial data, respectively. They assumed that the vulnerability of data is revealed by the closeness regarding either natural data or their adversarial variants. The definition of PM^{dif} is slightly different, which is the distance of a natural data point to its adversarial variant. PM^{dif} is viewed as a conceptual counterpart of LPS, but is critically different that it is continuous and path-independent. In our paper, we have verified the effectiveness of PM^{nat} and PM^{adv} and show that they can represent the geometric properties of data well. Note that, though these types of PM depict different geometric properties, they all share a negative correlation with the vulnerability of data—larger/smaller PMs indicate that the corresponding data are safer/riskier and thus should be assigned with smaller/larger weights during training.

Eventually, PM is employed for reweighting adversarial data during AT, where we propose the *margin-aware instance reweighting learning* (MAIL). With a non-decreased weight assignment function (cf. Eq. (8)), it pays much attention to those non-robust data. In experiments, MAIL is combined with various forms of commonly-used AT methods, including traditional AT [Madry et al., 2018], MART [Wang et al., 2020b], and TRADES [Zhang et al., 2019]. We demonstrate that PM is more reliable than previous works in geometric measurement, irrelevant to the forms of the adopted objectives. Moreover, in comparison with advanced methods, MAIL reveals its state-of-the-art performance against various attack methods, which benefit from our path-independent and continuous measurement.

2 Preliminary

2.1 Traditional Adversarial Training

For a K -classification problem, we consider a training dataset $S = \{(x_i, y_i)\}_{i=1}^n$ independently drawn from a distribution \mathcal{D} and a deep neural network $h(x; \theta)$ parameterized by θ . This deep classifier $h(x; \theta)$ predicts the label of an input data via $h(x; \theta) = \arg \max_k \mathbf{p}_k(x; \theta)$, with $\mathbf{p}_k(x; \theta)$ being the predicted probability (softmax on logits) of the k -th class.

The goal of AT is to train a model with a low adversarial risk regarding the distribution \mathcal{D} , i.e., $\mathcal{R}(\theta) = \mathbb{E}_{(x, y) \sim \mathcal{D}} [\max_{\delta \in \Delta} \ell(x + \delta, y; \theta)]$, where Δ is the threat model, defined by an L_p -norm bounded perturbation with the radius ϵ , i.e., $\Delta = \{\delta \in \mathbb{R}^d \mid \|\delta\|_p \leq \epsilon\}$. In the lens of statistical learning, we actually focuses on the empirical counterpart of $\mathcal{R}(\theta)$. In general, AT computes a new perturbation to update the model parameters, where the PGD method [Madry et al., 2018] is commonly adopted: for a (natural) example x_i , it starts with random noise ξ and repeatedly computes

$$\delta_i^{(t)} \leftarrow \text{Proj} \left[\delta_i^{(t-1)} + \alpha \text{sign} \left(\nabla_{\theta} \ell(x_i + \delta_i^{(t-1)}, y_i; \theta) \right) \right], \quad (1)$$

with Proj the clipping operation such that $\delta^{(t)}$ is always in Δ and sign the signum function. Due to non-convexity, we approximate the optimal solution by $\delta_i^{(T)}$ with T being the maximally allowed iterations.

Accordingly, $\delta_i^{(T)}$ is viewed as the perturbation for the *most* adversarial example [Zhang et al., 2021], and the learning objective function is formulated by

$$\arg \min_{\theta} \sum_i \ell(x_i + \delta_i^{(T)}, y_i; \theta). \quad (2)$$

Intuitively, AT corresponds to the *worst-case robust optimization*, continuously augmenting the training dataset with adversarial variants that highly confuse the current model. Therefore, it is a practical learning framework to alleviate the impact of adversarial attacks. However, it leads to insufficient network capacity, resulting in unsatisfactory model performance regarding adversarial robustness. The reason is that AT has an overwhelming smoothing effect in fitting highly adversarial examples [Zhang et al., 2019], and thus consumes a large model capacity to learn from individual data points.

2.2 Geometry-Aware Adversarial Training

Zhang et al. [2021] claimed that training examples should have unequal significance in AT, and proposed the *geometry-aware instance-reweighted adversarial training* (GAIRAT). It is a general framework to reweight adversarial data during training, where the Eq. (2) is modified as

$$\arg \min_{\theta} \sum_i \omega_i \ell(x_i + \delta_i^{(T)}, y_i; \theta) \quad \text{s.t. } \omega_i \geq 0 \text{ and } \sum_i \omega_i = 1. \quad (3)$$

The generation of the perturbation still follows Eq. (1). They suggested that data near the decision boundary are much vulnerable and should be assigned with large weights.

LPS as a geometric measurement. In assigning weights, GAIRAT requires a proper measurement for the distance. They suggested the estimation in high-dimensional input space via LPS (cf. Fig. 2), which is the least PGD iterations for a perturbation that leads to a wrong prediction. Intuitively, a small LPS indicates that the data point can quickly cross the decision boundary and thus close to it.

The drawbacks of LPS. Although promising results have been verified, LPS is path-dependent and limited by a few discrete values, where the consequence is non-negligible. In Figure 1(a), we showed that the PGD method will get stuck, resulting in that, using LPS as a geometric measurement, we might identify non-robust examples as robust ones during AT. Here, we modified the vanilla PGD method with the *line-searched* learning rate [Yu et al., 1995] and *Nesterov momentum* [Nesterov, 1983] (cf. Appendix A), termed *line-search & momentum-PGD* (LM-PGD), and we compared the loss curve of PGD with that of LM-PGD on one example. The maximal iterations of PGD was 50, and it is clear that, at the 14-th step, PGD almost converges, and the loss value does not ascend anymore. As a result, LPS of this example is 50, and this example is the most robust one in the view of LPS. However, LM-PGD still ascends after the 14-th step and successfully attacks such an instance at the 15-th step. This result means that such an instance is *not* a robust one, but LPS makes an wrong judgment regarding its robustness. The main reason is that LPS is heavily dependent on attack paths, even though both paths are highly similar.

We then demonstrate that the limited range of LPS would cause problems as well. In Figure 1b, we drew the histogram of LPSs for data in CIFAR-10 [Krizhevsky et al., 2009]. Higher LPS values mean that these examples are more robust and should be assigned smaller weights during AT. It can be seen that LPS has a confusing meaning when it equals the maximal value, which is 10 following [Madry et al., 2018]. For data whose LPSs are 10, they would be the most robust/safe ones. However, it can be seen that they still contain the critical data (the blue part). Although the proportion of the critical data seems low, ignoring them during AT (i.e., assigning small weights for them) will cause a significant problem: the accuracy of the trained classifier will drop significantly when facing the CW attack [Carlini and Wagner, 2017] (Figure 1c).

3 Probabilistic Margins for Instance Reweighting

The shortcomings of LPS motivate us to improve the measurement in discerning robust data and risky data, and we introduce our proposal in this section.

3.1 Geometry Information in view of Probabilistic Margin

Instead of using the input space as LPS, we suggest the measurement on estimated class-posterior probabilities, which are normalized embedding features (softmax on logits) in the range $[0, +1]$ for each dimension. Note that, without normalization, average distances from different classes might be of diverse scales (e.g., the average distance is 10 for the i -th class and 100 for the j -th class), increasing the challenge in comparing data from different classes.

Inspired by the *multi-class margin* in margin theory [Koltchinskii et al., 2002], we propose the *probabilistic margin* (PM) regarding the model outputs, namely,

$$\text{PM}(x, y; \theta) = \mathbf{p}_y(x; \theta) - \max_{j, j \neq y} \mathbf{p}_j(x; \theta), \quad (4)$$

where the first term in the r.h.s. is the *closeness* of x to the “center” of the true label y and the second term is the closeness to the nearest class except y (i.e., the most confusing label). The difference between the two terms is clearly a valid measurement, where the magnitude reflects the distance from the nearest boundary, and the signum indicates which side the data point belongs to. Figure 3 summarizes the key concepts, with i for the true label y and j for the most confusing class. For example, when $\mathbf{p}_y(x; \theta) = \mathbf{p}_j(x; \theta) = 0.5$, PM is 0 and the data point x is on the decision boundary between two classes; when $\mathbf{p}_y(x; \theta) = 0.6$ and $\mathbf{p}_j(x; \theta) = 0.4$, PM is positive and the data point x is much closer to the true label; if $\mathbf{p}_y(x; \theta) = 0.4$ and $\mathbf{p}_j(x; \theta) = 0.6$, PM is negative and the data point x is much closer to the most confusing class.

The above discussion indicates that PM can point out which geometric area a data point belongs to, where we discuss the following three scenarios: the *safe area* with large positive PMs, the *class-boundary-around data* with positive PMs close to 0, and the *wrong-prediction area* with negative PMs. The safe area contains guarded data that are insensitive to perturbation, which are safe and require low attention in AT (i.e., small weights); for data in the class-boundary-around data, they are much vulnerable to be attacked [Zhang et al., 2019, 2021] and thus need larger weights than the safe data; moreover, for data in the wrong-prediction area, they are the most critical since the attack method can successfully fool the current model, and thus they should be assigned the largest weights. This indicates a negative correlation of PM with vulnerability, where a larger PM requires a smaller weight.

In realization, the measurement of PM can be employed for adversarial data or natural ones, which are of the forms:

$$\text{PM}_i^{\text{adv}} = \mathbf{p}_{y_i}(x_i + \delta_i^{(T)}; \theta) - \max_{j, j \neq y_i} \mathbf{p}_j(x_i + \delta_i^{(T)}; \theta), \quad (5)$$

and

$$\text{PM}_i^{\text{nat}} = \mathbf{p}_{y_i}(x_i; \theta) - \max_{j, j \neq y_i} \mathbf{p}_j(x_i; \theta), \quad (6)$$

for a data point x_i , respectively. They assume that the vulnerability of data are revealed by the closeness regarding either natural data or their adversarial variants. Besides this two basic cases, one can also consider

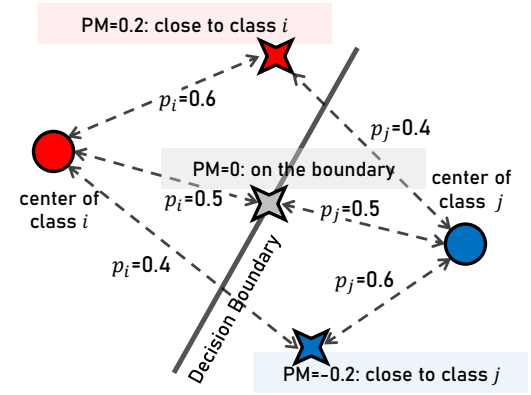


Figure 3: An illustration of PM, where p_i is the probability for the i -th class. As a special case, here we have $\text{PM} = p_i - p_j$ with i the target y and j the nearest class except y .

the data point x is on the decision boundary between two classes; when $\mathbf{p}_y(x; \theta) = 0.6$ and $\mathbf{p}_j(x; \theta) = 0.4$, PM is positive and the data point x is much closer to the true label; if $\mathbf{p}_y(x; \theta) = 0.4$ and $\mathbf{p}_j(x; \theta) = 0.6$, PM is negative and the data point x is much closer to the most confusing class.

The above discussion indicates that PM can point out which geometric area a data point belongs to, where we discuss the following three scenarios: the *safe area* with large positive PMs, the *class-boundary-around data* with positive PMs close to 0, and the *wrong-prediction area* with negative PMs. The safe area contains guarded data that are insensitive to perturbation, which are safe and require low attention in AT (i.e., small weights); for data in the class-boundary-around data, they are much vulnerable to be attacked [Zhang et al., 2019, 2021] and thus need larger weights than the safe data; moreover, for data in the wrong-prediction area, they are the most critical since the attack method can successfully fool the current model, and thus they should be assigned the largest weights. This indicates a negative correlation of PM with vulnerability, where a larger PM requires a smaller weight.

In realization, the measurement of PM can be employed for adversarial data or natural ones, which are of the forms:

$$\text{PM}_i^{\text{adv}} = \mathbf{p}_{y_i}(x_i + \delta_i^{(T)}; \theta) - \max_{j, j \neq y_i} \mathbf{p}_j(x_i + \delta_i^{(T)}; \theta), \quad (5)$$

and

$$\text{PM}_i^{\text{nat}} = \mathbf{p}_{y_i}(x_i; \theta) - \max_{j, j \neq y_i} \mathbf{p}_j(x_i; \theta), \quad (6)$$

for a data point x_i , respectively. They assume that the vulnerability of data are revealed by the closeness regarding either natural data or their adversarial variants. Besides this two basic cases, one can also consider

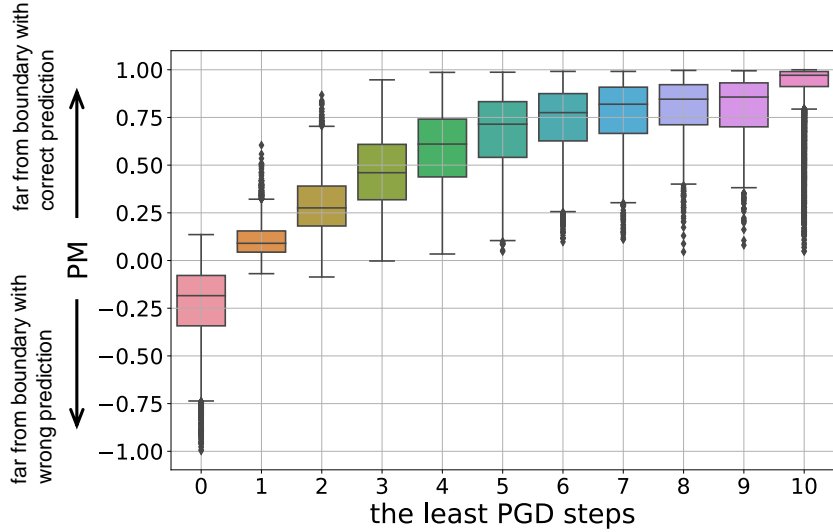


Figure 4: Comparison of LPS and PM (PM^{nat}). An interquartile range box represents the middle 50% of the considered data with the inside line being the median; a whisker is the range for the bottom/top 5% data, and points above/below whiskers are outliers.

the difference between the natural and adversarial predictions, namely,

$$\text{PM}_i^{\text{dif}} = \mathbf{p}_{y_i}(x_i; \theta) - \mathbf{p}_{y_i}(x_i + \delta_i^{(t_i)}; \theta), \quad (7)$$

where $t_i \leq T$ denotes LPS of x_i . PM^{dif} is a conceptual counterpart of LPS, while Eq. (7) is actually path-independent and continuous, which is more reliable than LPS. Note that, the valid range of PM^{dif} (i.e., $[0, +1]$) is different from that of PM^{adv} and PM^{nat} (i.e., $[-1, +1]$). It would bring unnecessary troubles since the geometric meanings of PM^{nat} and PM^{dif} are highly similar. Therefore, in experiments, we mainly verify the effectiveness of PM^{adv} and PM^{nat} .

Without direct involvement of the PGD method, PM is continuous and path-independent, making it more reliable than previous works, e.g., LPS. Now, we can further verify the drawbacks of LPS in view of the PM. In Figure 4, we depicted the box plot regarding PM for training data with various LPSs. The instability of LPS is evident: from the box centers, there is a little differentiation for data with large LPSs (e.g., LPS = 7 or 9) regarding PM; from the whiskers and outliers, the spreads of PMs are relatively scattered and the numbers of outliers are significant, confirming that the geometric messages characterized by LPS may not be very stable.

3.2 Margin-Aware Instance Reweighting Learning (MAIL)

To benchmark our proposal against state-of-the-art counterparts, we propose the *margin-aware instance reweighting learning* (MAIL). The overall algorithm is summarized in Algorithm 1. Generally, the objective is $\sum_i \omega_i \ell(x_i + \delta_i^{(T)}, y_i; \theta) + \mathcal{R}(x_i, y_i; \theta)$, where \mathcal{R} is an optional regularization term. This objective implies the optimization for the model, with one step (Step 5–8) generating adversarial variants, one step (Step 9–11) calculating importance weights, and one step (Step 12) minimizing the reweighted loss w.r.t. the model parameters.

Weight Assignment: We adopt the sigmoid function for weight assignment, which can be viewed as a *softened* sample selection operation of the form:

$$\omega_i^{\text{unn}} = \text{sigmoid}(-\gamma(\text{PM}_i - \beta)), \quad (8)$$

Algorithm 1 MAIL: The Overall Algorithm.

Input: a network model with the parameters θ ; and a training dataset S of size n .

Output: a robust model with parameters θ^* .

```

1: for  $e = 1$  to num_epoch do
2:   for  $b = 1$  to num_batch do
3:     sample a mini-batch  $\{(x_i, y_i)\}_{i=1}^m$  from  $S$ ; ▷ mini-batch of size  $m$ .
4:     for  $i = 1$  to batch_size do
5:        $\delta_i^{(0)} = \xi$ , with  $\xi \sim \mathcal{U}(0, 1)$ ;
6:       for  $t = 1$  to  $T$  do
7:          $\delta_i^{(t)} \leftarrow \text{Proj} \left[ \delta_i^{(t-1)} + \alpha \text{sign} \left( \nabla_{\theta} \ell(x_i + \delta_i^{(t-1)}, y_i; \theta) \right) \right]$ ;
8:       end for
9:        $w_i^{\text{unn}} = \text{sigmoid}(-\gamma(\text{PM}_i - \beta))$ ;
10:      end for
11:       $\omega_i = M \times w_i^{\text{unn}} / \sum_j w_j^{\text{unn}}$ ,  $\forall i \in [m]$ ; ▷  $\omega_i = 1$  during burn-in period.
12:       $\theta \leftarrow \theta - \eta \nabla_{\theta} \sum_{i=1}^m \omega_i \ell(x_i + \delta_i, y_i; \theta) + \mathcal{R}(x_i, y_i; \theta)$ ;
13:    end for
14:  end for

```

where β indicates how many data should have relatively large weights and $\gamma \geq 0$ controls the smoothness around β . Note that, PM_i denotes the PM score for the i -th data point, which could be any one of PM_i^{adv} , PM_i^{nat} , and PM_i^{dif} . Eq. (8) is a monotonic function that assigns large values for data with small PMs, paying attention to critical data as discussed in Section 2.2. Moreover, it should be further normalized by $\omega_i = N \times w_i^{\text{unn}} / \sum_j w_j^{\text{unn}}$ to meet the constraint in Eq. (3).

Burn-in Period: During the initial training phase, the geometric information is less informative since the deep model is not adequately learned. Directly using the computed weights may mislead the training procedure and accumulate the bias in erroneous weight assignment. Therefore, we introduce a burn-in period at the beginning, where ω is fixed to 1 regardless of the PM value. A similar strategy has also been considered in [Zhang et al., 2021].

Two Realizations: The MAIL is general for reweighting adversarial data, which could be combined with existing works. Here we give two representative examples: the first one is based on the vanilla AT [Wang et al., 2020b], with the learning objective of the form (termed MAIL-AT):

$$-\sum_i \omega_i \log \mathbf{p}_{y_i}(x_i + \delta_i^{(T)}; \theta). \quad (9)$$

The second one is based on TRADES [Zhang et al., 2019], which adopts the Kullback-Leibler (KL) divergence regarding natural and adversarial prediction, and also requires the learning guarantee (taken as a regularization term here) on the natural prediction. Overall, the learning objective is (termed MAIL-TRADES), given by

$$\beta \sum_i \omega_i \text{KL}(\mathbf{p}(x_i + \delta_i^{(T)}; \theta) \parallel \mathbf{p}(x_i; \theta)) - \sum_i \log \mathbf{p}_{y_i}(x_i; \theta), \quad (10)$$

where $\beta > 0$ is the trade-off parameter and $\text{KL}(p \parallel q) = \sum_k p_k \log p_k / q_k$ denotes the KL divergence regarding p and q .

Our proposal is flexible and general enough to be combined with many other advanced methods. For example, we can modify MART [Wang et al., 2020b], which could discern correct/wrong prediction, to further utilize their geometric properties (termed MAIL-MART). Its formulation is similar to that of MAIL-TRADES with a slightly different learning objective, which is listed in Appendix C.

Table 1: Comparison of LPS and PM on CIFAR-10 dataset.

	AT [Madry et al., 2018]			MART [Wang et al., 2020b]			TRADES [Zhang et al., 2019]		
	LPS	PM _{nat}	PM _{adv}	LPS	PM _{nat}	PM _{adv}	LPS	PM _{nat}	PM _{adv}
NAT	82.26 ± 0.60	82.50 ± 0.20	83.15 ± 0.46	84.45 ± 0.17	83.75 ± 0.09	84.12 ± 0.46	78.52 ± 0.20	82.71 ± 0.52	80.49 ± 0.18
PGD	54.14 ± 0.15	55.00 ± 0.32	55.25 ± 0.23	53.16 ± 0.26	53.63 ± 0.21	53.65 ± 0.23	51.67 ± 0.54	52.37 ± 0.65	53.67 ± 0.14
AA	36.32 ± 0.57	44.25 ± 0.45	44.10 ± 0.21	46.00 ± 0.26	46.70 ± 0.10	47.20 ± 0.21	44.40 ± 0.20	49.52 ± 0.11	49.54 ± 0.51

4 Experiments

We conducted extensive experiments on various datasets, including SVHN [Netzer et al., 2011], CIFAR-10 [Krizhevsky et al., 2009], and CIFAR-100 [Krizhevsky et al., 2009]. The adopted backbone models are ResNet (ResNet-18) [He et al., 2016] and wide ResNet (WRN-32-10) [Zagoruyko and Komodakis, 2016]. In Section 4.2, we verified the effectiveness of PM as a geometric measurement. In Section 4.3, we benchmarked our MAIL against advanced methods.

4.1 Experimental Setup

Training Parameters. For all considered methods, the networks were trained using (mini-batch) stochastic gradient descent with momentum 0.9, weight decay 3.5×10^{-3} (for ResNet-18) / 7×10^{-4} (for WRN-32-10), batch size 128, and initial learning rate 0.01 (for ResNet-18) / 0.1 (for WRN-32-10) which is divided by 10 at the 75-th and 90-th epoch. To some extent, this setup can alleviate the impact of adversarial over-fitting [Pang et al., 2020, Wang et al., 2020b]. Moreover, following [Madry et al., 2018], the perturbation bound ϵ is 8/255 and the (maximal) number of PGD steps k is 10 with step size $\alpha = 2/255$.

Hyperparameters. The slope and bias parameters were set to 30 and -0.07 in MAIL-AT and to 5 and 0.05 in both MAIL-TRADES and MAIL-MART. The trade-off parameter β was set to 5 in MAIL-TRADES, while it was 6 in MAIL-MART (cf. Algorithm 4 in Appendix C). For the training procedure, the weights started to update when the learning rate dropped at the first time following [Zhang et al., 2021], i.e., the initial 74 epochs is burn-in period, and then we employed the reweighted objective.

Robustness Evaluation. We evaluated our methods and baselines using the standard accuracy on natural test data (NAT) and the adversarial robustness based on several representative attack methods, including the PGD method with 100 iterations [Madry et al., 2018], CW attack [Carlini et al., 2019], APGD CE attack (APGD), and adaptive attack (AA). All these methods have full access to the model parameters (i.e., *white-box* attacks) and are constrained by the same perturbation limit as above. Note that, here we do not focus on the *black-box* attack methods [Bai et al., 2020, Cheng et al., 2019, Li et al., 2020, 2019], which are relatively easy to be defensed [Chakraborty et al., 2018].

4.2 Effectiveness of probabilistic Margin

In this section, we verified the effectiveness of PM as a measurement in comparison with LPS. Here, we adopted ResNet-18 as the backbone and conducted experiments on CIFAR-10 dataset.

Three representative methods were considered, including AT [Madry et al., 2018], MART [Wang et al., 2020b], and TRADES [Zhang et al., 2019], which were further reweighted by assigned weights given by either PM or LPS [Zhang et al., 2021]. For LPS, we adopted the weight assignment function in GAIRAT with the suggested setup [Zhang et al., 2021]. We remind that AT-LPS, MART-LPS, and TRADES-LPS represent GAIRAT, GAIR-MART, and GAIR-TRADES in [Zhang et al., 2021]; and AT-PM, MART-PM,

Table 2: Average accuracy (%) and standard deviation on CIFAR-10 dataset with ResNet-18.

	NAT	PGD	APGD	CW	AA
AT [Madry et al., 2018]	84.86 ± 0.17	48.91 ± 0.14	47.70 ± 0.06	51.61 ± 0.15	44.90 ± 0.53
TRADES [Zhang et al., 2019]	84.00 ± 0.23	52.66 ± 0.16	52.37 ± 0.21	52.30 ± 0.06	48.10 ± 0.26
MART [Wang et al., 2020b]	82.28 ± 0.60	53.50 ± 0.46	52.73 ± 0.57	51.59 ± 0.16	48.40 ± 0.14
FAT [Zhang et al., 2020]	87.97 ± 0.15	46.78 ± 0.12	46.68 ± 0.16	49.92 ± 0.26	43.90 ± 0.82
GAIRAT [Zhang et al., 2021]	83.22 ± 0.06	54.81 ± 0.15	50.95 ± 0.49	39.86 ± 0.08	33.35 ± 0.57
MAIL-AT	83.15 ± 0.46	55.25 ± 0.23	53.20 ± 0.38	47.81 ± 0.11	44.10 ± 0.21
MAIL-TRADES	81.84 ± 0.18	53.68 ± 0.14	52.92 ± 0.62	52.89 ± 0.31	50.03 ± 0.51

and TRADES-PM represent MAIL-AT, MAIL-MART, and MAIL-TRADES, respectively. Note that, we mainly validated two types of PM here, namely, PM_{adv} and PM_{nat} that which are very different from LPS.

The experimental results with 5 individual trials are summarized in Table 1, where we adopted three representative evaluations, including natural performance (NAT), the PGD method with 100 steps (PGD), and adaptive attack (AA). Note that AA can be viewed as an ensemble of several advanced attacks (e.g., CW and APGD) and thus reliably reflect the adversarial robustness. As we can see, the superiority of PM is apparent, regardless of the adopted learning objectives: the results of PM are 0.70-7.93% better than LPS regarding AA and 0.14-2.00% better regarding PGD. Although LPS could achieve comparable results regarding PGD attacks, its adversarial robustness is quite low when facing AA attacks. It indicates that the robustness improvement of GAIRAT might be partially. This is probably caused by *obfuscated gradients* [Athalye et al., 2018a], since stronger attack methods (e.g., AA) lead to poorer performance on adversarial robustness.

Moreover, comparing the results in using PM_{nat} and PM_{adv} , both PMs can lead to promising robustness, while PM_{adv} is slightly better. The reason is that PM_{adv} can precisely describe the distance between adversarial variants and decision boundaries. As a result, it can help accurately assign important instances high weights during AT. Therefore, we adopt PM_{adv} in the following experiments.

4.3 Performance Evaluation

Now, we benchmarked our proposal against state-of-the-art methods in the literature. Here, we mainly report the results on the CIFAR-10 dataset due to the space limitation. For the results on other datasets, please refer to Appendix B.

Compared Baselines. We compared the proposed method with the following baselines: (1) (traditional) AT [Madry et al., 2018]: the cross-entropy loss for adversarial perturbation generated by the PGD method; (2) TRADES [Zhang et al., 2019]: a learning objective with an explicit trade-off between the adversarial and natural performance; (3) MART [Wang et al., 2020b]: a training strategy which treats wrongly/correctly predicted data separately; (4) FAT [Zhang et al., 2020]: adversarial training with early-stopping in adversarial intensity; (5) GAIRAT [Zhang et al., 2021]: geometric-aware instance-reweighted adversarial training.

All the methods were run for 5 individual trials with different random seeds, where we reported their

Table 3: Average accuracy (%) and standard deviation on CIFAR-10 dataset with WRN-32-10.

	NAT	PGD	APGD	CW	AA
AT	87.80	49.43	49.12	53.38	48.46
	± 0.13	± 0.29	± 0.26	± 0.05	± 0.46
TRADES	86.36	54.88	55.02	56.18	53.40
	± 0.52	± 0.39	± 0.27	± 0.16	± 0.37
MART	84.76	55.61	55.40	54.72	51.40
	± 0.34	± 0.51	± 0.37	± 0.20	± 0.05
FAT	89.70	48.79	48.72	52.39	47.48
	± 0.17	± 0.18	± 0.36	± 0.89	± 0.30
GAIRAT	86.30	58.74	55.64	45.57	40.30
	± 0.61	± 0.46	± 0.36	± 0.18	± 0.16
MAIL-AT	84.83	58.86	55.82	51.26	47.10
	± 0.39	± 0.25	± 0.31	± 0.20	± 0.22
MAIL-TRADES	84.00	57.40	56.96	56.20	53.90
	± 0.15	± 0.96	± 0.19	± 0.30	± 0.22

average accuracy and standard deviation. The results are summarized in Table 2 and Table 3 with the backbone models being ResNet-18 and WRN-32-10, respectively. Overall, our MAIL achieved the best or the second-best robustness against all four types of attacks, revealing the superiority of MAIL (i.e., MAIL-AT and MAIL-TRADES) in adversarial robustness. Specifically, AT and TRADES both treat training data equally, and the results were unsatisfactory compared with the best one (0.55% – 6.34% decline with ResNet-18 and 0.02% – 9.43% decline with WRN – 32 – 10), which imply the possibility for their further improvements. Though MART and FAT consider the impact of individuals on the final performance, they fail in paying attention to non-robust data during training. Concretely, MART mainly focuses on the correctness regarding natural prediction, and FAT prevents the model learning from *highly* non-robust data in keeping its natural performance. Therefore, FAT achieved the best natural performance (3.11% – 6.13% improvement with ResNet-18 and 1.90% – 5.70% improvement with WRN-32-10), while its robustness against adversaries seems inadequate (2.97% – 8.45% decline with ResNet-18 and 3.81%-10.07% decline with WRN-32-10). Moreover, in adopting LPS as the geometric measurement, GAIRAT performed well regarding PGD and AGPD attacks, but the adversarial robustness on CW and AA attacks were low. In comparison, we retain the supremacy on PGD-based attacks (i.e., PGD and APGD) as in GAIRAT and reveal excellent performance on CW and AA attacks. For example, in Table 2, we achieved 0.44%-8.47% improvements on PGD attack, 0.47%-6.52% on APGD attack, 0.59%-13.03% on CW attack, and 1.63%-16.68% on AA attack.

MAIL-AT performs well on PGD-based methods, while MAIL-TRADES is good at CW and AA attacks. It suggests that the robustness depends on adopted learning objectives, coinciding with the previous conclusion in [Wang et al., 2020b]. In general, we suggest using MAIL-TRADES as a default choice, as it reveals promising results regarding AA while keeping a relatively high performance regarding PGD. Besides, comparing the results in Table 2 and Table 3, the overall accuracy had a promising improvement in employing models with a much large capacity (i.e., WRN-32-10), partially verifying the fact that deep models still have insufficient network capacity in fitting adversarial variants [Zhang et al., 2021].

5 Conclusion

In this paper, we focus on boosting adversarial robustness by reweighting adversarial data during training, where data closer to the current decision boundaries are more critical and thus require larger weights. To measure the closeness, we suggest the use of PM, which relates to the multi-class margin regarding the probabilistic space of model outputs (i.e., the estimated class-posterior probabilities). Without any involvement of the PGD iterations, PM is continuous and path-independent and thus overcomes the drawbacks of previous works (e.g., LPS) efficaciously. Moreover, we consider several types of PMs with different geometric properties, and propose a general framework termed MAIL. Experiments demonstrated that PMs are more reliable measurements than previous works, and our MAIL revealed its superiority against state-of-the-art methods, independent of adopted (basic) learning objectives. In the future, we will delve deep into the mechanism in instance-reweighted adversarial learning, theoretically study the contribution of individuals for the final performance, and improve the methodology in using geometric characteristics of data.

References

Maksym Andriushchenko and Nicolas Flammarion. Understanding and improving fast adversarial training. In *NeurIPS*, 2020.

Anish Athalye, Nicholas Carlini, and David A. Wagner. Obfuscated gradients give a false sense of security: Circumventing defenses to adversarial examples. In *ICML*, 2018a.

Anish Athalye, Logan Engstrom, Andrew Ilyas, and Kevin Kwok. Synthesizing robust adversarial examples. In *ICML*, 2018b.

Yang Bai, Yuyuan Zeng, Yong Jiang, Yisen Wang, Shu-Tao Xia, and Weiwei Guo. Improving query efficiency of black-box adversarial attack. In *ECCV*, 2020.

Sébastien Bubeck, Yin Tat Lee, Eric Price, and Ilya P. Razenshteyn. Adversarial examples from computational constraints. In *ICML*, 2019.

Nicholas Carlini and David A. Wagner. Towards evaluating the robustness of neural networks. In *S&P*, 2017.

Nicholas Carlini, Anish Athalye, Nicolas Papernot, Wieland Brendel, Jonas Rauber, Dimitris Tsipras, Ian Goodfellow, Aleksander Madry, and Alexey Kurakin. On evaluating adversarial robustness. *arXiv preprint arXiv:1902.06705*, 2019.

Anirban Chakraborty, Alam Manaar, Dey Vishal, Chattopadhyay Anupam, and Mukhopadhyay Debdeep. Adversarial attacks and defences: A survey. *arXiv preprint arXiv:1810.00069*, 2018.

Tianlong Chen, Sijia Liu, Shiyu Chang, Yu Cheng, Lisa Amini, and Zhangyang Wang. Adversarial robustness: From self-supervised pre-training to fine-tuning. In *CVPR*, 2020.

Minhao Cheng, Thong Le, Pin-Yu Chen, Huan Zhang, Jinfeng Yi, and Cho-Jui Hsieh. Query-efficient hard-label black-box attack: An optimization-based approach. In *ICLR*, 2019.

Corinna Cortes and Vladimir Vapnik. Support-vector networks. *Machine learning*, 20(3):273–297, 1995.

Daniel Cullina, Arjun Nitin Bhagoji, and Prateek Mittal. Pac-learning in the presence of evasion adversaries. *arXiv preprint arXiv:1806.01471*, 2018.

Marcos Lopez De Prado. *Advances in financial machine learning*. John Wiley & Sons, 2018.

Xuefeng Du, Jingfeng Zhang, Bo Han, Tongliang Liu, Yu Rong, Gang Niu, Junzhou Huang, and Masashi Sugiyama. Learning diverse-structured networks for adversarial robustness. In *ICML*, 2021.

Alhussein Fawzi, Seyed-Mohsen Moosavi-Dezfooli, Pascal Frossard, and Stefano Soatto. Empirical study of the topology and geometry of deep networks. In *CVPR*, 2018.

Samuel G Finlayson, John D Bowers, Joichi Ito, Jonathan L Zittrain, Andrew L Beam, and Isaac S Kohane. Adversarial attacks on medical machine learning. *Science*, 363(6433):1287–1289, 2019.

Ruize Gao, Feng Liu, Jingfeng Zhang, Bo Han, Tongliang Liu, Gang Niu, and Masashi Sugiyama. Maximum mean discrepancy is aware of adversarial attacks. In *ICML*, 2021.

Kaiming He, Xiangyu Zhang, Shaoqing Ren, and Jian Sun. Deep residual learning for image recognition. In *CVPR*, 2016.

Andrew Ilyas, Shibani Santurkar, Dimitris Tsipras, Logan Engstrom, Brandon Tran, and Aleksander Madry. Adversarial examples are not bugs, they are features. In *NeurIPS*, 2019.

Vladimir Koltchinskii, Dmitry Panchenko, et al. Empirical margin distributions and bounding the generalization error of combined classifiers. *Annals of statistics*, 30(1):1–50, 2002.

Alex Krizhevsky, Geoffrey Hinton, et al. Learning multiple layers of features from tiny images. 2009.

Alexey Kurakin, Ian J. Goodfellow, and Samy Bengio. Adversarial examples in the physical world. In *ICLR*, 2017.

Jie Li, Rongrong Ji, Hong Liu, Jianzhuang Liu, Bineng Zhong, Cheng Deng, and Qi Tian. Projection & probability-driven black-box attack. In *CVPR*, 2020.

Yandong Li, Lijun Li, Liqiang Wang, Tong Zhang, and Boqing Gong. NATTACK: learning the distributions of adversarial examples for an improved black-box attack on deep neural networks. In *ICML*, 2019.

Geert Litjens, Thijs Kooi, Babak Ehteshami Bejnordi, Arnaud Arindra Adiyoso Setio, Francesco Ciompi, Mohsen Ghafoorian, Jeroen Awm Van Der Laak, Bram Van Ginneken, and Clara I Sánchez. A survey on deep learning in medical image analysis. *Medical image analysis*, 42:60–88, 2017.

Aleksander Madry, Aleksandar Makelov, Ludwig Schmidt, Dimitris Tsipras, and Adrian Vladu. Towards deep learning models resistant to adversarial attacks. In *ICLR*, 2018.

Yu Nesterov. A method of solving a convex programming problem with convergence rate $o(1/k^2)$. In *Sov. Math. Dokl.*, 1983.

Yuval Netzer, Tao Wang, Adam Coates, Alessandro Bissacco, Bo Wu, and Andrew Y Ng. Reading digits in natural images with unsupervised feature learning. 2011.

Tianyu Pang, Xiao Yang, Yinpeng Dong, Hang Su, and Jun Zhu. Bag of tricks for adversarial training. *arXiv preprint arXiv:2010.00467*, 2020.

Yao Qin, Nicholas Carlini, Garrison W. Cottrell, Ian J. Goodfellow, and Colin Raffel. Imperceptible, robust, and targeted adversarial examples for automatic speech recognition. In *ICML*, 2019.

Ludwig Schmidt, Shibani Santurkar, Dimitris Tsipras, Kunal Talwar, and Aleksander Madry. Adversarially robust generalization requires more data. In *NeurIPS*, 2018.

Christian Szegedy, Wojciech Zaremba, Ilya Sutskever, Joan Bruna, Dumitru Erhan, Ian J. Goodfellow, and Rob Fergus. Intriguing properties of neural networks. In *ICLR*, 2014.

Dimitris Tsipras, Shibani Santurkar, Logan Engstrom, Alexander Turner, and Aleksander Madry. Robustness may be at odds with accuracy. In *ICLR*, 2019.

Haotao Wang, Tianlong Chen, Shupeng Gui, Ting-Kuei Hu, Ji Liu, and Zhangyang Wang. Once-for-all adversarial training: In-situ tradeoff between robustness and accuracy for free. In *NeurIPS*, 2020a.

Yisen Wang, Difan Zou, Jinfeng Yi, James Bailey, Xingjun Ma, and Quanquan Gu. Improving adversarial robustness requires revisiting misclassified examples. In *ICLR*, 2020b.

Eric Wong, Leslie Rice, and J. Zico Kolter. Fast is better than free: Revisiting adversarial training. In *ICLR*, 2020.

Shuo Yang, Tianyu Guo, Yunhe Wang, and Chang Xu. Adversarial robustness through disentangled representations. In *AAAI*, 2021.

Xiao-Hu Yu, Guo-An Chen, and Shixin Cheng. Dynamic learning rate optimization of the backpropagation algorithm. *IEEE Trans. Neural Networks*, 6(3):669–677, 1995.

Sergey Zagoruyko and Nikos Komodakis. Wide residual networks. In *BMVC*, 2016.

Hongyang Zhang, Yaodong Yu, Jiantao Jiao, Eric P. Xing, Laurent El Ghaoui, and Michael I. Jordan. Theoretically principled trade-off between robustness and accuracy. In *ICML*, 2019.

Jingfeng Zhang, Xilie Xu, Bo Han, Gang Niu, Lizhen Cui, Masashi Sugiyama, and Mohan S. Kankanhalli. Attacks which do not kill training make adversarial learning stronger. In *ICML*, 2020.

Jingfeng Zhang, Jianing Zhu, Gang Niu, Bo Han, Masashi Sugiyama, and Mohan Kankanhalli. Geometry-aware instance-reweighted adversarial training. In *ICLR*, 2021.

Yuli Zheng, Zhenyu Wu, Ye Yuan, Tianlong Chen, and Zhangyang Wang. Pcal: A privacy-preserving intelligent credit risk modeling framework based on adversarial learning. *arXiv preprint arXiv:2010.02529*, 2020.

A Line-Search & Momentum-PGD

Here, we describe the detailed realization of the Line-Search & Momentum-PGD method. Compared with the commonly used PGD method of the form following

$$\delta_i^{(t)} \leftarrow \text{Proj} \left[\delta_i^{(t-1)} + \alpha \text{sign} \left(\nabla_{\theta} \ell(x_i + \delta_i^{(t-1)}, y_i; \theta) \right) \right], \quad (11)$$

the Line-Search & Momentum-PGD makes two improvements: (1) we use the Nesterov gradient [Nesterov, 1983] in an attempt to overcome the sub-optimal points, i.e.,

$$v_i^{(t)} \leftarrow \gamma v_i^{(t-1)} + \alpha^{(t-1)} \text{sign} \left(\nabla_{\theta} \ell(x_i + \delta_i^{(t-1)}, y_i; \theta) \right), \quad (12)$$

$$\delta_i^{(t)} \leftarrow \text{Proj} \left[\delta_i^{(t-1)} + v_i^{(t)} \right], \quad (13)$$

where γ is the momentum parameter and $\alpha^{(t)}$ is the step size at the t -th iteration; (2) and we adopt the line-searched step size [Yu et al., 1995], which aims at finding the optimal $\alpha^{(t-1)}$ in a predefined searching space $V = [\alpha^{(\min)}, \alpha^{(\max)}]$, namely

$$\alpha^{(t-1)} \leftarrow \arg \max_{\alpha \in V} \ell \left(x_i + \text{Proj} \left[\delta_i^{(t-1)} + \gamma v_i^{(t-1)} + \alpha \text{sign} \left(\nabla_{\theta} \ell(x_i + \delta_i^{(t-1)}, y_i; \theta) \right) \right], y_i; \theta \right). \quad (14)$$

In Figure 1(a), the maximal PGD iteration is 50, with γ being 0.8, α^{\max} being 6/255, and α^{\min} being 4/255 in the first 15 iterations and 0 otherwise.

B Further Experiments

To further demonstrate the robustness of our proposal against adversarial attacks, we also conducted experiments on SVHN [Netzer et al., 2011] and CIFAR-100 [Netzer et al., 2011] datasets. Here we adopted ResNet-18 as the backbone model with the same experimental setup as in Section 4.2, where we reported the natural accuracy (NAT), PGD-20 attack (PGD), and adaptive attack (AA). All the experiments are conducted for 5 individual trials, and the average performance and standard deviations are summarized in Table 4. All the methods were realized by Pytorch 1.81¹ with CUDA 11.1², where we used GeForce RTX 3090 GPU and AMD Ryzen Threadripper 3960X Processor. On average, it takes about 8 hours for a trial for our method.

Some advanced methods (e.g., TRADES and MART) can hardly beat the traditional AT on these two datasets, indicating the performance of the learning methods may also depend on the considered datasets. Moreover, FAT retains the highest natural performance (i.e., NAT) but its results on PGD and AA are relatively low, which are similar to Table 2 and Table 3. For GAIRAT on CIFAR-100, we observe that its performance on the PGD attack was not as high as some other datasets (e.g., SVHN and CIFAR-10), it may reveal that the deficiencies of LPS are non-negligible for some difficult tasks. There may exist some better reweighting strategies in boosting adversarial robustness. As we can see, our MAIL-AT and MAIL-TRADES, which benefit from the proposed PM, achieved the best or the comparable (e.g., AA on CIFAR-100) performance regarding various adversarial attacks, and the natural accuracy retained to be acceptable.

B.1 Further Discussion

We adopt an instance-reweighting learning framework and propose PMs in measuring the robustness regarding adversarial attacks. Our PMs are continuous and path-independent, overcoming the deficiency of previous

¹<https://pytorch.org/>

²<https://developer.nvidia.com/>

Table 4: Average test accuracy (%) and standard deviation (5 trials) on SVHN and CIFAR-100.

	SVHN			CIFAR-100		
	NAT	PGD	AA	NAT	PGD	AA
AT	93.55 ± 0.65	54.76 ± 0.30	46.58 ± 0.46	60.13 ± 0.39	28.69 ± 0.24	24.76 ± 0.25
TRADES	93.65 ± 0.29	55.12 ± 0.68	45.74 ± 0.31	60.73 ± 0.33	29.83 ± 0.25	24.90 ± 0.33
MART	92.57 ± 0.14	55.45 ± 0.26	43.52 ± 0.43	54.08 ± 0.60	29.94 ± 0.21	25.30 ± 0.50
FAT	93.68 ± 0.31	53.81 ± 0.77	41.68 ± 0.49	66.74 ± 0.28	23.25 ± 0.55	20.88 ± 0.13
GAIRAT	90.47 ± 0.77	64.67 ± 0.26	37.00 ± 0.30	58.43 ± 0.28	25.74 ± 0.51	17.54 ± 0.33
MAIL-AT	93.68 ± 0.25	65.54 ± 0.16	41.12 ± 0.30	60.74 ± 0.15	27.62 ± 0.27	22.44 ± 0.53
MAIL-TRADES	89.68 ± 0.19	58.40 ± 0.21	49.10 ± 0.22	60.13 ± 0.25	30.28 ± 0.19	24.80 ± 0.25

works [Zhang et al., 2021]. The overall method is general and flexible, combined with existing works to boost their primary performance.

Moreover, there is still room for improvement in our approach and related works. This paper mainly focuses on adversarial robustness regarding white-box attacks generated by the first-order gradient-based methods. When employing our MAIL in real-world applications, it may lead to over-confidence regarding many other attacks, e.g., verified attacks, black-box attacks, and physical attacks. It poses the potential risk and dangers for the resulting systems (e.g., autonomous driving), as it would produce non-robust behavior unexpectedly when encountering unseen types of attacks.

The problems of fairness should also be considered since individuals are not treated equally during training. For data assigned with larger weights, the resulting model would be more robust when encounters similar data during the test. This unfairness problem seems inevitable for a reweighted learning framework, which will interest our further study. Moreover, our method might be more vulnerable to error-prone data (e.g., with label noise) than traditional AT since MAIL would provide abnormal weights (e.g., larger weights than expectation) for these data. This issue would mislead the training procedure in fitting *noise*, which has an apparent negative impact on the model.

C Realizations of MAIL

In this section, we provide the detailed algorithms for our three realizations, namely, MAIL-AT (in Algorithm 2), MAIL-TRADES (in Algorithm 3), and MAIL-MART (in Algorithm 4). In Algorithm 4, the *boosted cross entropy* (BCE) loss is of the form:

$$\text{BCE}(x_i + \delta_i^{(T)}, y_i; \theta) = -\log \mathbf{p}_{y_i}(x_i + \delta_i^{(T)}) - \log(1 - \max_{k \neq y_i} \mathbf{p}_k(x_i + \delta_i^{(T)})), \quad (15)$$

where the first term in the r.h.s. is the common cross entropy loss and the second term is a regularization term that make the prediction much confident. The *mis-classification aware KL* (MKL) term is of the form:

$$\text{MKL}(x_i, \delta_i^{(T)}; \theta) = \text{KL}(\mathbf{p}(x_i + \delta_i^{(T)}; \theta) || \mathbf{p}(x_i; \theta))(1 - \mathbf{p}_{y_i}(x_i; \theta)), \quad (16)$$

which reweights the KL-divergence by the estimated probability of a correct prediction.

Algorithm 2 MAIL-AT: The Overall Algorithm.

Input: a network model with the parameters θ ; and a training dataset S of size n .

Output: a robust model with parameters θ^* .

```

1: for  $e = 1$  to num_epoch do
2:   for  $b = 1$  to num_batch do
3:     sample a mini-batch  $\{(x_i, y_i)\}_{i=1}^m$  from  $S$ ;                                 $\triangleright$  mini-batch of size  $m$ .
4:     for  $i = 1$  to batch_size do
5:        $\delta_i^{(0)} = \xi$ , with  $\xi \sim \mathcal{U}(0, 1)$ ;
6:       for  $t = 1$  to  $T$  do
7:          $\delta_i^{(t)} \leftarrow \text{Proj} \left[ \delta_i^{(t-1)} + \alpha \text{sign} \left( \nabla_{\theta} - \log \mathbf{p}_{y_i}(x_i + \delta_i^{(t-1)}; \theta) \right) \right]$ ;
8:       end for
9:        $w_i^{\text{unn}} = \text{sigmoid}(-\gamma(\text{PM}_i - \beta))$ ;
10:      end for
11:       $\omega_i = M \times w_i^{\text{unn}} / \sum_j w_j^{\text{unn}}$ ,  $\forall i \in [m]$ ;                       $\triangleright \omega_i = 1$  during burn-in period.
12:       $\theta \leftarrow \theta - \eta \nabla_{\theta} \left( -\sum_{i=1}^m \omega_i \log \mathbf{p}_{y_i}(x_i + \delta_i^{(T)}; \theta) \right)$ ;
13:    end for
14:  end for

```

Algorithm 3 MAIL-TRADES: The Overall Algorithm.

Input: a network model with the parameters θ ; and a training dataset S of size n .

Output: a robust model with parameters θ^* .

```

1: for  $e = 1$  to num_epoch do
2:   for  $b = 1$  to num_batch do
3:     sample a mini-batch  $\{(x_i, y_i)\}_{i=1}^m$  from  $S$ ;                                 $\triangleright$  mini-batch of size  $m$ .
4:     for  $i = 1$  to batch_size do
5:        $\delta_i^{(0)} = \xi$ , with  $\xi \sim \mathcal{U}(0, 1)$ ;
6:       for  $t = 1$  to  $T$  do
7:          $\delta_i^{(t)} \leftarrow \text{Proj} \left[ \delta_i^{(t-1)} + \alpha \text{sign} \left( \nabla_{\theta} \text{KL}(\mathbf{p}(x_i + \delta_i^{(t-1)}; \theta) \parallel \mathbf{p}(x_i; \theta)) \right) \right]$ ;
8:       end for
9:        $w_i^{\text{unn}} = \text{sigmoid}(-\gamma(\text{PM}_i - \beta))$ ;
10:      end for
11:       $\omega_i = M \times w_i^{\text{unn}} / \sum_j w_j^{\text{unn}}$ ,  $\forall i \in [m]$ ;                       $\triangleright \omega_i = 1$  during burn-in period.
12:       $\theta \leftarrow \theta - \eta \nabla_{\theta} \sum_i \left( \beta \omega_i \text{KL}(\mathbf{p}(x_i + \delta_i^{(T)}; \theta) \parallel \mathbf{p}(x_i; \theta)) - \sum_i \log \mathbf{p}_{y_i}(x_i; \theta) \right)$ ;
13:    end for
14:  end for

```

Algorithm 4 MAIL-MART: The Overall Algorithm.

Input: a network model with the parameters θ ; and a training dataset S of size n .

Output: a robust model with parameters θ^* .

```

1: for  $e = 1$  to num_epoch do
2:   for  $b = 1$  to num_batch do
3:     sample a mini-batch  $\{(x_i, y_i)\}_{i=1}^m$  from  $S$ ;                                 $\triangleright$  mini-batch of size  $m$ .
4:     for  $i = 1$  to batch_size do
5:        $\delta_i^{(0)} = \xi$ , with  $\xi \sim \mathcal{U}(0, 1)$ ;
6:       for  $t = 1$  to  $T$  do
7:          $\delta_i^{(t)} \leftarrow \text{Proj} \left[ \delta_i^{(t-1)} + \alpha \text{sign} \left( \nabla_{\theta} - \log \mathbf{p}_{y_i}(x_i + \delta_i^{(t-1)}; \theta) \right) \right]$ ;
8:       end for
9:        $w_i^{\text{unn}} = \text{sigmoid}(-\gamma(\text{PM}_i - \beta))$ ;
10:      end for
11:       $\omega_i = M \times w_i^{\text{unn}} / \sum_j w_j^{\text{unn}}$ ,  $\forall i \in [m]$ ;                       $\triangleright \omega_i = 1$  during burn-in period.
12:       $\theta \leftarrow \theta - \eta \nabla_{\theta} \left( - \sum_{i=1}^m \omega_i \text{BCE}(x_i + \delta_i^{(T)}, y_i; \theta) + \beta \text{MKL}(x_i, \delta_i^{(T)}; \theta) \right)$ ;
13:    end for
14:  end for

```
